Improved Photophysical Properties of Ionic Material-Based Combination Chemo/PDT Nanomedicine

Samantha Macchi,

Department of Chemistry, University of Arkansas at Little Rock, Little Rock, Arkansas 72204, United States

Mohd Zubair,

Department of Biology, University of Arkansas at Little Rock, Little Rock, Arkansas 72204, United States

Robert Hill,

Department of Chemistry, University of Arkansas at Little Rock, Little Rock, Arkansas 72204, United States

Nabeel Alwan,

Department of Chemistry, University of Arkansas at Little Rock, Little Rock, Arkansas 72204, United States

Yusuf Khan,

Department of Electrical and Computer Engineering, University of Texas at Austin, Austin, Texas 78712, United States

Nawab Ali,

Department of Biology, University of Arkansas at Little Rock, Little Rock, Arkansas 72204, United States

Grégory Guisbiers,

Department of Physics and Astronomy, University of Arkansas at Little Rock, Little Rock, Arkansas 72204, United States

Brian Berry,

Department of Chemistry, University of Arkansas at Little Rock, Little Rock, Arkansas 72204, United States

Noureen Siraj

Department of Chemistry, University of Arkansas at Little Rock, Little Rock, Arkansas 72204, United States

Corresponding Author Noureen Siraj – Department of Chemistry, University of Arkansas at Little Rock, Little Rock, Arkansas 72204, United States; Phone: (501) 916-6544; nxsiraj@ualr.edu.

Abstract

Herein, a cost-effective and prompt approach to develop ionic material-based combination nanodrugs for cancer therapy is presented. A chemotherapeutic (phosphonium) cation and photodynamic therapeutic (porphyrin) anion are combined using a single step ion exchange reaction. Afterward, a nanomedicine is prepared from this ionic materials-based combination drug using a simplistic strategy of reprecipitation. Improved photophysical characteristics such as a slower nonradiative rate constant, an enhanced phosphorescence emission, a longer lifetime, and a bathochromic shift in absorbance spectra of porphyrin are observed in the presence of a chemotherapeutic countercation. The photodynamic therapeutic activity of nanomedicines is investigated by measuring the singlet oxygen quantum yield using two probes. As compared to the parent porphyrin compound, the synthesized combination material showed a 2-fold increase in the reactive oxygen species quantum yield, due to inhibition of face-to-face aggregation of porphyrin units in the presence of bulky chemotherapeutic ions. The dark cytotoxicity of combination therapy nanomedicines in the MCF-7 (cancerous breast) cell line is also increased as compared to their corresponding parent compounds in vitro. This is due to the high cellular uptake of the combination nanomedicines as compared to that of the free drug. Further, selective toxicity toward cancer cells was acquired by functionalizing nanomedicine with folic acid followed by incubation with MCF-7 and MCF-10A (noncancerous breast). Light toxicity experiments indicate that the synthesized ionic nanomedicine shows a greater cell death than either parent drug due to the improved photophysical properties and effective combination effect. This facile and economical strategy can easily be utilized in the future to develop many other combination ionic nanomedicines with improved photodynamics.

Graphical Abstract
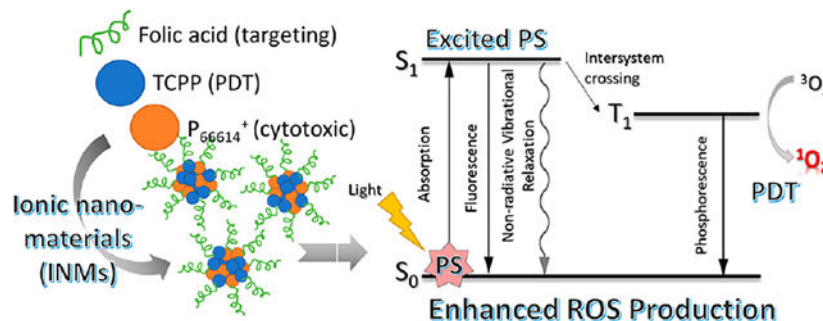
Keywords

ionic liquids; cytotoxicity; ionic materials; photodynamic therapy; porphyrin

1. INTRODUCTION

Cancer is currently the second leading cause of death in the world, only behind heart disease. In the United States, the death toll is projected to be 606 520 people (2020), making up nearly 22% of overall deaths.[1] Commonly utilized therapies such as chemotherapy, radiation, and surgery are highly invasive with extreme side effects for the patient.

Therefore, the development of new cancer therapy practices is of utmost importance. One promising method to treat cancer is the use of combination therapy. In combination therapy, two or more therapeutic mechanisms are combined in a single drug to improve the anticancer effects as compared to one method alone. Furthermore, this approach potentially minimizes harmful side effects and combats drug resistance by using a lower dose of each drug/treatment.[2] There are numerous potential combinations of drugs and treatments, but one that has gained particular interest in recent years is the tandem use of chemotherapy and photodynamic therapy (PDT).[3,4] For the effective treatment of advanced cancer, the Food and Drug Administration (FDA) has approved several combinations of medication.[5,6] However, currently available combination drugs are costly due to their complicated synthesis protocol.[7-9] Therefore, it is imperative to develop new economical drugs using a simple, rapid, and inexpensive approach with advanced properties. In this study, a new class of compounds is introduced, that is, ionic materials (IMs), to develop a combination therapy medicine.

IMs, sometimes called frozen ionic salts, are a subclass of ionic liquids (ILs) and share many of the same characteristics, except that they are solids at room temperature.[10] The main reason for their low melting point is the presence of bulky, long chain, often organic ions, which makes the packing of ions less efficient due to steric hindrance. These materials are highly thermally stable and tunable in their chemical and photophysical properties. Therefore, they have been explored for multiple applications.[11-17] ILs are highly tunable where both counterions can be easily exchanged to fit specific applications. The cationic nitrogen and phosphorus-based ILs have gained attention in regards to their chemotherapeutic activity.[18-21] Some of the ILs show cytotoxicity toward normal cells, which has restricted their use for medical applications. In this project, for the first time, a chemo–PDT combination nanomedicine from IMs was developed.

Many recent advances in cancer research seek to address the undesirable toxicity of chemotherapeutic agents toward normal cells. It is evident that nanomaterials have shown greater potential in cancer research for several reasons, including greater cellular uptake and enhanced permeability and retention (EPR) phenomenon.[22-24] This has led to the use of nanoparticles (NPs) due to their increased intracellular concentration in cancer cells and lower toxicity in normal cells.[25-27] Many inorganic NPs including heavy metals, metal oxides, and quantum dots have been developed for cancer therapy.[28,29] These toxic, nonbiodegradable inorganic NPs may cause detrimental effects on normal cells.[30,31] Therefore, organic NPs are currently attracting considerable attention among researchers due to their excellent biocompatibility, biodegradability, and nontoxicity.[32-34] In this regard, IMs are highly applicable in the field of cancer research due to their ability to form ionic nanomaterials (INMs) where room-temperature ILs can form nanodroplets, which are not true NPs and are often unstable. In this study, carrier free INMs without the use of any matrix are presented for the first time as combination therapy nanomedicines for cancer.

Cancer nanodrugs are also commonly surface-functionalized with targeting agents to enhance the selective toxicity of the drugs toward cancer cells. This technique can also alter the cellular uptake mechanism by adding receptor-mediated uptake routes. Some promising molecules used for coating drugs include polymers, specific antibodies, and

small molecules, etc.[35,36] Folic acid (FA) is a common small molecule targeting agent as it has been shown that folate receptors are overexpressed in certain types of solid tumors in breast, lung, and epithelial tissues.[37] Mostly, folic acid moieties are covalently attached to drugs to enhance selective toxicity toward cancer cells.[38] However, this is a complex, timeconsuming, costly, and low yield methodology. Therefore, it is of utmost importance to seek a simple and cost-effective strategy to functionalize the surface of NPs. In the present study, a porphyrin-based combination nanomedicine's surface is coated with folate using ionic and intermolecular interactions.

An effective photosensitizer (PS) is of critical importance for effective PDT. An ideal PS possesses several characteristics such as absorption wavelength maxima at longer wavelength to treat deeper seated tumors in the body, high singlet oxygen quantum yield, high molar absorptivity, and no dark toxicity. Porphyrin molecules are very well studied in terms of their application in PDT.[29,39,40] Previous work using porphyrin-based INMs showed enhanced photophysical properties as PDT PSs.[41,42] Several studies have been performed to improve the PDT efficiency of porphyrin by inhibiting aggregation in the planar structure of porphyrin.[30,40,42] A simplistic approach to improve photophysical properties is acquired by replacing the small counterion of porphyrin with a bulky moiety to prevent face aggregation that would otherwise reduce the PDT efficiency of the drug.

In this study, a chemotherapeutic phosphonium cation, trihexyltetradecylphoshonium (P_{66614}^+), is paired with a photosensitizing anion, *meso*-tetra(4-carboxyphenyl)porphyrin ($TCPP^{4-}$), to produce a single molecule IM, the tetra-(trihexyltetradecylphosphonium) *meso*-tetrakis(4-carboxyphenyl)porphyrin ($[P_{66614}]_4[TCPP]$) combination drug. This chemotherapeutic and photodynamic therapeutic (chemo–PDT) IM is a hydrophobic compound, which can easily be converted to INMs in aqueous/buffer solution via reprecipitation.[41,42] These INMs are highly tunable, and their surface charge is altered by functionalization with folate to enhance cellular uptake and selective cytotoxicity toward cancerous cells. INMs' surface charge and hydrodynamic radius are also determined. The photophysical properties of the parent porphyrin compound (TCPP), IMs ($[P_{66614}]_4[TCPP]$), and its INMs are studied in detail to investigate their potential as a PDT nanodrug. The singlet oxygen quantum yield is also investigated using a probe to determine the PDT activity of the IMs. The cytotoxicity of the carrier-free nanodrugs, before and after functionalization with folate, is investigated in vitro using two cell lines (cancerous and noncancerous cells). To the best of our knowledge, this is the first report where the ILs chemistry approach has been used to develop combination therapeutic nanomedicines for cancer therapy application.

2. MATERIALS AND METHODS

2.1. Chemicals.

Trihexyltetradecylphosphonium chloride ($P_{66614}Cl$) was purchased from Sigma-Aldrich (St. Louis, MO), and porphyrin (TCPP) was purchased from Tokyo Chemical Industry (Tokyo, Japan). FA was purchased from Calbiochem (San Diego, CA). 1,3-Diphenylisobenzofuran (DPBF) and 9,10-anthracenediylbis(methylene)dimalonic acid (ABDA) were purchased from Sigma-Aldrich. Sodium hydroxide and methylene blue (MB) were purchased from

VWR (Radnor, PA). All chemicals were used as received, and only TCPP was modified prior to the IMs synthesis. Triply deionized water (18.2 MΩ cm) was obtained using a Purelab Ultrapure water purification system (ELGA, Woodridge, IL). Dichloromethane (DCM) and ethanol were of ACS grade and purchased from Thermo Fisher (Waltham, MA). MTT (3-(4,5-dimethylthiazol-2-yl)-2,5-diphenyltetrazolium bromide) and PBS buffer (pH 7.4) and dimethyl sulfoxide (DMSO) were purchased from Sigma-Aldrich. DMSO was filtered through a 0.2 μm polytetrafluoroethylene (PTFE) filter prior to use.

2.2. Synthesis and Characterization of IMs for Combination Cancer Therapy.

The combination therapy drug was synthesized from two parent compounds utilizing a simple, rapid, economical one-step ion exchange method. $P_{66614}Cl$ was used as the chemotherapeutic compound, and TCPP acted as the PDT drug (Figure 1). Solution A was prepared by dissolving $P_{66614}Cl$ in DCM. Solution B was prepared by deprotonation of TCPP with 6 mol equiv of sodium hydroxide in water. This mixture was allowed to stir for 30 min to ensure full deprotonation of all four carboxylic protons. Aqueous solution B of 1 mol equiv of sodium salt of TCPP (Na_4TCPP) was then added to a reaction vessel containing 4 mol equiv of solution A (in DCM) in a 1:2 v/v ratio. The reaction vessel was stirred for 24 h to ensure complete ion exchange. Later, the water layer containing sodium chloride salt was discarded, and the organic layer was washed three times with water to remove any remaining salt. The organic solvent layer was then dried via rotary evaporation to remove the DCM, and the resultant drug, $[P_{66614}]_4[TCPP]$, was collected, freeze-dried to remove moisture, and used for further studies. The combination drug was characterized using electrospray ionization mass spectrometry (ESI–MS), which was performed using a Bruker (Billerica, MA) Ultraflex 9.4T in methanol solvent. The mass-to-charge ratio peaks in positive and negative ion mode verified the presence of both the cation and the anion in $[P_{66614}]_4[TCPP]$ (Figures S1 and S2). Nuclear magnetic resonance (NMR, JEOL) was used to verify the purity of $[P_{66614}]_4[TCPP]$. ^1H NMR (400 MHz, $(CD_3)_2SO$): δ −2.88 (s, 2H), 0.84 (m, 48H), 1.27 (q, 192H), 2.15 (t, 32H), 8.08 (d, 8H), 8.25 (d, 8H), 8.84 (s, 8H). The NMR spectra are given in Figure S3.

2.3. Synthesis and Characterization of INMs for Combination Cancer Therapy.

INMs were prepared by reprecipitation in water or cell media from the IMs' stock solution in ethanol for spectroscopic measurements and in DMSO for cellular studies, respectively. Briefly, a stock solution of the combination drug was prepared at 1 mM concentration in ethanol or DMSO and was dropwise added to a scintillation vial of deionized water/cell media already present in an active sonication bath. The vial was allowed to sonicate for 15 min with a 30 min rest period prior to the measurements. For FA-functionalized INMs, a stock solution of chemo–PDT IM in DMSO was added dropwise to a 100 μM solution of FA under sonication in the same manner as mentioned earlier for INM synthesis. FA-INMs were recovered by centrifugation. A NanoBrook 90PLUS (Brookhaven Instruments Corp., Holtsville, NY) was used to determine the zeta potential and hydrodynamic diameter of the INMs in DI water using the dynamic light scattering method (DLS). Transmission electron microscopy (TEM) imaging was performed to characterize the INMs size using a JEOL FEI Tecnai F20 200 keV microscope. $[P_{66614}]_4[TCPP]$ INMs were prepared for TEM analysis by dropwise addition of 0.1 mL of IM stock solution in 0.9 mL of water under sonication

followed by 30 min rest and subsequent centrifugation to concentrate the particles. INMs were resuspended in water, and then 4 μL was drop-casted onto the grids. Lacey carbon grids (Ted Pella, Redding, CA) were used for TEM imaging.

2.4. Photophysical Properties.

The absorption and fluorescence emission spectra of the parent compounds, the synthesized IMs, and the INMs for combination cancer therapy were recorded and analyzed. A UV–visible spectrometer (Agilent Cary 5000, Santa Clara, CA) and fluorometer (Horiba Fluorolog, Kyoto, Japan) were used to record the absorption and emission spectra, respectively. Starna quartz cuvettes with four sides and 1 cm path length were used for the fluorescence/phosphorescence emission measurements. Quantum yield measurements were performed using a relative method with TCPP as a standard in ethanol. The quantum yields of the IMs and INMs were determined in ethanol solvent using eq 1.

$$\Phi_{un} = \Phi_s \times \frac{I_{un}}{I_s} \times \frac{Abs_s}{Abs_{un}} \times \left(\frac{n_{un}}{n_s}\right)^2 \tag{1}$$

where Φ_s is the quantum yield of the standard, I is the integrated fluorescence emission intensity, Abs is the absorbance at the excitation wavelength, and n is the refractive index of the standard (n_s) and unknown (n_{un}). Radiative and nonradiative rate constants were also calculated from the photophysical data. From the absorbance and emission spectra, the radiative rate constant was calculated (k_{rad}) using the Stricker–Berg relationship (eq 2).

$$k_{rad} = 2.88 \times 10^{-9} \times n^2 \times \frac{\int I(\tilde{\nu})\,d\tilde{\nu}}{\int I(\tilde{\nu})\tilde{\nu}^{-3}\,d\tilde{\nu}} \int \frac{\varepsilon(\tilde{\nu})}{\tilde{\nu}}\,d\tilde{\nu} \tag{2}$$

where I is the emission intensity, ν is the wavenumber of light, and ε is the molar extinction coefficient. The radiative rate constant was used to determine the nonradiative rate constant (k_{nonrad}) from eq 3.

$$\Phi_F = \frac{k_{rad}}{k_{rad} + k_{nonrad}} \tag{3}$$

Fluorescence lifetimes were recorded using the time correlated single photon counting (TCSPC) method with a DeltaHub controller in conjunction with a Horiba fluorometer. A NanoLED (Horiba) source (1 MHz, 390 nm excitation wavelength) was used as an excitation source. Data were processed with DAS6 software using exponential fitting of raw data. Phosphorescence emission was recorded using a 0.1 ms delay time at low temperature (77 K). Phosphorescence decay was performed using the Decay by Delay method and fit using one exponential.

2.5. Reactive Oxygen Species and Singlet Oxygen Generation Measurements.

The reactive oxygen species (ROS) quantum yield of the parent TCPP and [P$_{66614}$]$_4$[TCPP] chemo–PDT combination IMs was investigated to determine the efficiency of the PDT drug. The obtained results for the parent and IMs were compared to investigate the changes in

PDT performance of the porphyrin drug when converted into combination cancer therapy IMs. DPBF was used as a ROS probe, and ABDA was used as a singlet oxygen selective probe. DPBF is yellow in ethanol solution with an absorption maximum wavelength at 411 nm. The probe is oxidized by singlet oxygen and other ROS, which disrupts its conjugated system and converts it into a transparent solution (cannot absorb light).[42] Similarly, the ABDA probe exhibits a decrease in absorbance at a wavelength maximum of 380 nm when reacted with singlet oxygen in water. In a typical experiment with DPBF, TCPP and the IM derived from TCPP were dissolved in ethanol, separately. DPBF then was dissolved in the same solvent and added to each drug solution separately with a final concentration of 5 μM drug in 100 μM DPBF. The rate of ROS produced was quantified by irradiating the solution at the wavelength maxima of TCPP and IMs (417 nm) for 60 s time intervals and a total irradiation time of 420 s using a fluorescence spectrofluorometer (14 nm slit) and then measuring the absorption spectra of the solution using a UV visible spectrophotometer. The ROS produced during irradiation of TCPP/IMs was scavenged by DPBF. After each irradiation treatment, changes in the absorbance intensity of DPBF at 411 nm were monitored using a UV/vis spectrophotometer. MB was used as a standard to calculate the ROS quantum yield of the TCPP parent compound and of the IMs.

Using the ABDA probe, because it is not as sensitive as DBPF, the final concentration of the drug (TCPP or INMs) used was 10 μM, and the probe concentration was 200 μM in water. A similar irradiation protocol was followed as before, with slight modification. The solution was irradiated at 150 s intervals for a total time of 1200 s, and the absorbance decrease of ABDA was monitored at 380 nm upon reaction with singlet oxygen. The ROS and singlet oxygen quantum yield were calculated using eq 4.[43]

$$\Phi_{\Delta(x)} = \Phi_{\Delta(std)} \times \frac{S_x}{S_{std}} \times \frac{1 - 10^{-A_{std}}}{1 - 10^{-A_x}} \tag{4}$$

where S is the slope of the plot of probe absorbance versus time, A is the absorbance of sample without probe, subscript x is the unknown sample (TCPP or [P$_{66614}$]$_4$[TCPP]), and subscript std is the standard.[42]

The absorption maxima wavelengths of the probes (DPBF/ABDA) and of porphyrin are very close to each other. Thus, to prove that a decrease in absorption intensity is due to the probe reaction with ROS and not due to photobleaching of TCPP/IMs, another experiment was designed. In this experiment, only the TCPP/IMs/INMs solution without any singlet oxygen probe was irradiated using a fluorometer. A second control experiment was designed to ensure photobleaching of the probe was due to singlet oxygen produced by the standard or porphyrin alone. In this experiment, only the probe was irradiated under the same parameters of the previous experiment.

2.6. Cell Culture/Cell Viability.

Model human cell lines, MCF-7 cancerous cells, and MCF-10A noncancerous cells were purchased from American Type Culture Collection (ATCC, Manassas, VA). Dulbecco's modified Eagle's medium (DMEM), Trypsin-EDTA (0.25%), penicillin, streptomycin, and minimal essential medium were purchased from Caisson Lab (Smithfield, UT). Fetal

bovine serum (FBS) was obtained from Atlanta Biologicals (Lawrenceville, GA). Mammary epithelial cell basal medium, epidermal growth factor, insulin, hydrocortisone, bovine pituitary extract, gentamicin, and amphotericin B were all purchased from PromoCell (Heidelberg, DE). In vitro studies were performed using two cell lines, MCF-7 and MCF-10A. All cells were maintained in monolayer at 37 °C and 5% CO_2 in complete medium. MCF-7 cells were cultured in DMEM with phenol red, supplemented with FBS (10% v/v) and penicillin/streptomycin antibiotic solution (500 units/mL). MCF-10A cells were grown in mammary epithelial cell basal medium supplemented with epidermal growth factor (10 ng/mL), insulin (5 μg/mL), hydrocortisone (0.5 μg/mL), bovine pituitary extract (0.004 mL/mL), gentamicin (100 μg/mL), and amphotericin B (0.05 μg/mL). At the desired confluence, cells were subcultured by trypsinization, and detached cells were counted using a hemocytometer following staining with trypan blue exclusion dye.

To determine the 24 h dark toxicity, cells were seeded in 96-well plates at 10^4 cells per well and incubated at 37 °C (5% CO_2) for 24 h. Cells were then treated with different concentrations of drug for 24 h. INMs were prepared at various concentrations by diluting stock solution in cell culture media following bath sonication, while maintaining a sterile environment. DMSO used as a vehicle was at a maximum of 0.5% to avoid any cellular toxicity. Appropriate controls with complete media alone and vehicle control without drug (DMSO) were included. Following treatment, cells were washed with PBS buffer. MTT assay was used to determine the cell viability as described previously.[44] A microplate reader (Biotek Synergy H1, Winooski, VT) was used to determine the optical density at 570 nm for the MTT assay. For in vitro studies, each experiment was performed in triplicate and repeated three times. All data that show error bars are presented as mean ± standard deviation (SD) unless otherwise mentioned. The significance of difference in the mean values was determined using the two-tailed student "t" test. Values with significant difference are denoted as $*p < 0.05$, $**p < 0.01$, and $***p < 0.005$.

Light toxicity experiments were performed to determine the combination chemo–PDT effect intracellularly. Cells were treated in a manner similar to that described above. Briefly, 10^4 cells were plated in a 96-well plate and allowed to incubate 24 h. Afterward, cells were treated with INMs or TCPP and incubated again for 4 h. The media containing drug was removed, and the cells were washed thrice with PBS to remove the external drug. Cell media was replaced in each well, and the plate was irradiated with a visible lamp (0.14 W/cm^2) for 10 min. A control experiment was run in tandem with identical conditions but was not exposed to light. Following irradiation, the plate was incubated an additional 24 h, and MTT assay was used to determine the cell viability.

Cellular uptake experiments were performed to investigate the amount of TCPP or INMs taken up by MCF-7 cells at a given time interval. 3.0×10^5 cells were seeded in a six-well plate and incubated at 37 °C for 24 h. TCPP or INMs were added to each well at a final concentration of 2 μM (in 2 mL) and incubated in the dark for 4 h. After the allotted time, the cells were washed thoroughly with PBS three times to remove any external drug. Cells were dissolved with 3 mL of DMSO, and concentrations were determined by a UV–vis spectrophotometer.

3. RESULTS AND DISCUSSION

3.1. Drug Characterization.

Reprecipitation of combination cancer therapy IMs in water yielded spherical NPs, which are reported by TEM to be 24.2 ± 5.1 nm in diameter (Figure S4). The solvated diameter of the particles was analyzed using the DLS method in water and was found to be 45.2 ± 6.7 nm (Figure S5). This value is approximately double the value obtained for dry NPs due to biasing of DLS measurements by inherent weighting factors.[42] Upon coating with FA, the hydrodynamic diameter was further increased to 53.3 ± 12.5 nm, which proved the functionalization of INMs.

Zeta potential measurements were also performed for the NPs in water. The values of the zeta potential for combination INMs were determined to be $+33.5 \pm 4.7$ mV. This high positive zeta potential indicates the presence of majority bulky phosphonium cations at the surface of the INMs. The magnitude of the surface charge indicates a stable colloidal suspension of INMs in aqueous media. The positive surface charge of combination therapy nanomedicine may allow for enhanced preferential uptake by cells because the cellular membranes are negatively charged. Coating with FA yielded particles with a zeta potential value of $+17.2 \pm 2.5$ mV. This indicates that negatively charged FA altered the surface charge of the INMs combination drug, which further confirms the presence of folate ions at the surface of INMs.

3.2. Photophysical Characterization.

Absorbance spectra of the parent compound, TCPP, IM ($[P_{66614}]_4[TCPP]$), and $[P_{66614}]_4[TCPP]$ INMs were recorded and compared. All compounds show characteristic spectra of porphyrins that contain a Soret band at ~415–420 nm and of four Q-bands at approximately 515, 550, 590, and 650 nm (Figure 2a). An ethanolic solution of TCPP and $[P_{66614}]_4[TCPP]$ IMs shows similar wavelength maxima. However, a notable red shift in absorption maxima wavelength is observed for aqueous $[P_{66614}]_4[TCPP]$ INMs as compared to TCPP in water. The Soret band position of $[P_{66614}]_4[TCPP]$ INMs in water is slightly red-shifted from 415 to 420 nm as compared to the parent dye, free TCPP in water. The largest bathochromic shift in wavelength is observed at the longest wavelength Q-band from 638 to 652 nm. The shift of absorption maxima wavelength is highly desirable to attain a better penetration depth of light in bodily tissue. These results indicate that improved photophysical properties of porphyrin are attained by attaching a bulky chemotherapeutic cation in IMs and INMs. A slight decrease in molar extinction coefficient at the Soret band wavelength is observed for $[P_{66614}]_4[TCPP]$ INMs in water than for its parent dye in water (Table 1). This is attributed to the particle formation of combination therapy nanomedicines as compared to the soluble TCPP parent dye. In chemo–PDT INMs, porphyrin molecules are mostly present inside, and the surface is covered with an alkyl phosphonium ion (confirmed by a positive zeta potential), which does not absorb light. Moreover, those porphyrin anions reside at the outer layer that can absorb light, while the interaction of the inner molecule of porphyrin in NPs with electromagnetic radiation can be weak. The difference in molar extinction values at the Q bands for the TCPP and $[P_{66614}]_4[TCPP]$ compounds is much less than that for the Soret bands. It is observed that the photophysical properties of a

PDT drug are tuned by attaching four alkyl phosphonium chemotherapeutic cations. Thus, it is proved that ILs chemistry can be utilized to successfully tailor the photophysical properties of the PS used as PDT agent in combination cancer therapy. It is well-known that planar porphyrins like TCPP may aggregate at elevated concentrations.[45,46] Thus, aggregation experiments were conducted for aqueous TCPP and $[P_{66614}]_4[TCPP]$ INMs at concentrations up to 0.05 mM. It was found that TCPP shows an additional peak at approximately 440 nm at high concentrations (Figure S6), indicating a potential aggregation state.[47,48] No additional peak for INMs is seen at 0.05 mM, indicating that the introduction of a bulky phosphonium counterion effectively inhibits aggregation of TCPP units even at high concentration.

Upon coating the surface of INMs with FA, the functionalized INMs absorption spectrum remains similar in shape. The absorption peak maximum at 420 nm for the $[P_{66614}]_4[TCPP]$ INMs spectrum is slightly red-shifted to 425 nm when functionalized with FA (Figure S7). There is also significant broadening of the Soret band in the FA-coated INMs spectrum. As mentioned earlier, the longer wavelength absorption maxima are achieved in INMs when functionalized with FA, which is advantageous for PDT application because these nanomedicines can be used to treat a deeply seated tumor due to the ability of longer wavelength light to penetrate deeper into the body tissue.

Fluorescence measurements for porphyrin-based compounds show that the $[P_{66614}]_4[TCPP]$ INMs fluorescence emission intensity is reduced and red-shifted as compared to that of free TCPP in water (Figure 2b). A similar trend is observed in the absorption spectra of the aforementioned samples. Therefore, the fluorescence quantum yield and rate of decay (radiative and nonradiative) were investigated to predict the PS's performance in both compounds, which is directly corelated with the PDT efficiency.

3.3. Quantum Yield and Photophysical Rate Constants.

Fluorescence quantum yield measurements were performed to investigate the change in quantum yield upon conversion of porphyrin into IMs and INMs. In this experiment, TCPP was used as a standard compound as it shows absorption in a similar wavelength region. The quantum yields of the IMs and INMs were determined in ethanol solvent using eq 1. TCPP has a literature quantum yield value of 0.044 in ethanol, which is used as a standard here.[49] After deprotonation in water, the quantum yield is enhanced up to 0.058 (Table 2). This could be due to polarity-induced structural changes, commonly seen in fluorophores,[50] such as a lowered aggregation of the porphyrin unit in water as compared to that of ethanol. Aggregation can quench fluorescence and thus lead to lower quantum yields. Upon conversion of TCPP to IM, $[P_{66614}]_4[TCPP]$, the quantum yield is slightly higher than that of its parent compound with a value of 0.048 in ethanol solvent. This increase in quantum yield value is attributed to the presence of bulky phosphonium moieties, which minimized the aggregations of the porphyrin moieties in ethanol. However, INMs exhibited a lower fluorescence quantum yield as compared to that of the parent porphyrin compound, which indicates the chances of an improved intersystem crossing process that is essential to develop effective PDT nanomedicine. FA-INMs showed an even lower quantum yield of 0.016, which is indicative of other possible transitions.

The radiative and nonradiative rates were also investigated (using eqs 2 and 3) as these parameters can shed light on the PDT mechanism of the PSs. It is noteworthy that IM and INMs show slower radiative and nonradiative decay rates as compared to that of the parent compound (Table 2). Additionally, FA-INMs show a similar radiative rate constant as compared to that of INMs. The results of photophysical characterization suggest that there is a possibility of increased triplet state population in INMs, which can consequently enhance the PDT efficiency of INMs by converting molecular oxygen into singlet oxygen in the excited triplet state. Therefore, phosphorescence emission experiments are performed.

3.4.   Phosphorescence Emission Spectra.

The existence of a triplet excited state is a crucial requirement for a PDT drug to generate singlet oxygen species. The photodynamics of the triplet state can shed light on the PDT capability of a PS. The phosphorescence of TCPP and $[P_{66614}]_4[TCPP]$ was recorded separately in ethanol at 77 K. It was found that $[P_{66614}]_4[TCPP]$ shows much more intense phosphorescence emission as compared to its parent porphyrin at the same concentration (Figure S8). This further confirms the greater populated first excited triplet state (T_1) of IM as compared to that of TCPP.

3.5.   Photostability.

High photostability is an important criterion for a fluorophore when applying it practically in biological systems. The effect of a phosphonium cation on the photostability of TCPP was investigated by performing a kinetic study. It has been proven that the addition of an IL-based counterion improves the photostability of macrocyclic dye molecules (e.g., porphyrins and phthalocyanines).[41,42] The photostability of TCPP and $[P_{66614}]_4[TCPP]$ was determined over 1000 s after excitation at 420 nm and monitoring the emission in kinetic mode at 650 nm with a slit width of 14–14 nm. Both compounds exhibit excellent stability in ethanol solvent (Figure S9).

3.6.   Fluorescence and Phosphorescence Lifetime.

Fluorescence lifetimes of TCPP and $[P_{66614}]_4[TCPP]$ were measured in ethanol using TCSPC measurement. The decays were found to have a best fit of two exponentials. The lifetimes of both compounds are tabulated in Table 3. Most of the TCPP fluorescent species showed a 9.5 ns lifetime, while the $[P_{66614}]_4[TCPP]$ chemo–PDT IM major component exhibited a longer (10.5 ns) lifetime. These lifetimes are attributed to the first excited singlet states (S_1). This longer lived S_1 state has a greater chance to undergo intersystem crossing to T_1 where reaction with molecular oxygen can occur.

Phosphorescence lifetime is a crucial factor in the effectiveness of a molecule to produce ROS. Decays for TCPP and $[P_{66614}]_4[TCPP]$ were measured in ethanol at 77 K and fitted using the first exponential equation (Figure S10). Decays were found to be 0.006 and 0.25 ms for TCPP and $[P_{66614}]_4[TCPP]$, respectively, in ethanol solvent. Conversion of porphyrin into IM exhibited a longer phosphorescence lifetime around 2 orders of magnitude. The longer triplet state lifetime of $[P_{66614}]_4[TCPP]$ allows more time to react with triplet oxygen molecules present in the cells before relaxing through phosphorescence. These lifetime

results demonstrate the possibility of a higher ROS quantum yield of the IM and thus should show a greater PDT effect than TCPP.

3.7. ROS/Singlet Oxygen Quantum Yield.

The efficiency of a PDT drug is determined by calculating the ROS and singlet oxygen quantum yield values. Previously, both fluorescence and phosphorescence emission results indicated significant changes in the photophysical properties of the IM as compared to the TCPP. Thus, the generation of ROS in IMs is also likely to be affected. To investigate the efficiency of the PDT moiety in the combination drug, the ROS quantum yield of parent TCPP and $[P_{66614}]_4[TCPP]$ IMs is determined using an ROS scavenging probe, DPBF. Photodegradation of DPBF upon reaction with radical oxygen species is well-known and thus is a commonly used molecular probe for ROS detection.[51,52] DPBF is insoluble in water; therefore, the quantum yield of INMs in aqueous media was recorded later with the ABDA probe.[53] TCPP and $[P_{66614}]_4[TCPP]$ solutions in ethanol were prepared and used to investigate the ROS. DPBF is a radical scavenging molecule (yellow solution) that, upon selective reaction with ROS, is converted into 1,2-dibenzoylbenzene (colorless solution).[53,54] Thus, the photo-degradation can easily be analyzed by monitoring the decrease in absorbance of DPBF at 411 nm using a spectrophotometer.

A solution of sample mixed with DPBF in ethanol was irradiated every 60 s for a total of 420 s at an excitation wavelength of 417 nm (Figure 3a). ROS quantum yield, Φ , was determined for each sample using eq 4. The ROS quantum yield for the MB standard is 0.52 in ethanol solvent. The quantum yield value is doubled upon conversion of porphyrin into IM (Table 4). This is attributed to the presence of bulky phosphonium ions, which inhibit porphyrin face-to-face aggregation that is detrimental to the production of ROS.[55] It also verified that a longer lived triplet state, improved phosphorescence emission intensity, and lower fluorescence quantum yield aided to attain a high singlet oxygen quantum yield for the chemo–PDT combination drug based on IM as compared to the parent compound.

To determine the singlet oxygen generation of INMs in aqueous solution, ABDA probe was used as a selective singlet oxygen scavenger. While ABDA is more selective toward singlet oxygen as compared to other ROS, its sensitivity is much lower than that of DPBF.[56] Thus, longer irradiation intervals of 150 s were used, and the absorbance was monitored at 380 nm. It was found that INMs generated singlet oxygen with a much faster rate as compared to MB or TCPP (Figure 3b). These results demonstrated that the conversion of TCPP to IMs and INMs can greatly enhance their singlet oxygen quantum yield and thus their PDT efficiency. To confirm that the decrease in absorbance of the probe is due to the generation of singlet oxygen by the PS, a control experiment was designed where the probe alone was irradiated. No significant decrease was observed for the probe, indicating that INMs are generating sufficient singlet oxygen under irradiation (Figure S11).

3.8. In Vitro Cellular Toxicity of INMs and Cellular Uptake.

After detailed characterization of the newly developed combination IM and INMs, these materials were tested in vitro for their potential application as combination cancer therapy drugs. In this regard, human breast cancer cell line MCF-7 was selected, and the half

maximal inhibitory concentration (IC_{50}) of the drug was compared to its counterpart noncancerous human breast cell line MCF-10A to determine the specificity of the drug toward cancerous cells. MTT assay was used to assess the cell viability as a result of cytotoxic effects in the above-mentioned cell lines incubated with $[P_{66614}]_4[TCPP]$ INMs, $(P_{66614})Cl$, and the TCPP parent molecule. All experiments were performed in 96-well plates with 10^4 cells per well in triplicate to ensure replicable data. Statistical significance was determined by using a two-tailed student's t test. To study the concentration-dependent cytotoxicity, cells were incubated with 0.5–20 μM of chemotherapeutic molecule and combination nanodrug for 24 h followed by MTT assay.

The IC_{50} value of the drug was analyzed by plotting the log of cell viability versus the concentration of drug and applying an exponential fit. It was shown that among both cell lines used, the parent porphyrin molecule (TCPP) was not cytotoxic under the concentration range tested. For other drugs, the toxicity increased with an increase in concentration as expected. It is important to note that the combination drug contains four chemotherapeutic moieties per molecule, while the parent compound contains only one. However, the cytotoxicity of $[P_{66614}]_4[TCPP]$ in the MCF-7 cell line is only about 2 times lower than the parent value (Table 5). This is attributed to the formation of stable NPs for the combination drug that have a different uptake mechanism as compared to that of the parent molecule. The cell viability for each drug as a function of concentration in MCF-7 and MCF-10A cells is shown in Figures 4a and S12, respectively.

The FA-functionalized INMs, which are shown in the literature to improve selectivity toward tumors, due to overexpression of FA receptors in many types of cancer cells,[36,57] can also aid in nondestructive and targeted delivery of NPs to cancer cells.[58] FA-functionalized INMs are labeled as FA-$[P_{66614}]_4[TCPP]$. The IC_{50} value of FA-$[P_{66614}]_4[TCPP]$ in the cancer cell line was found to increase as compared to that of the non-FA-coated INMs (Figure 4b), which could be due to the large solvated radius of the FA-INMs that can affect passive uptake by EPR phenomenon less favorably.[59] However, the IC_{50} value of the FA-coated INMs in the noncancerous cell line (MCF-10A) was greater than that of the same drug in the MCF-7 cells (Table 5). The FA-functionalized INMs showed selectivity toward cancer cells that was not observed for either drug without FA functionalization at the surface of NPs. This represents an easy and efficient approach to produce low-cost selective nanodrugs with combination mechanisms for cancer treatment.

The dark in vitro studies validate the improved cytotoxicity of chemo–PDT INMs. Moreover, enhanced selective toxicity toward cancerous cells was attained by functionalizing the INMs with FA. It should be noted that dark cytotoxicity results only account for the role of the chemotheraputic ion in the combination INMs, whereas the counteranion of INMs can add its toxicity mechanism only upon light irradation. To validate the dual mechanism (chemo–PDT) in vitro, light cytotoxicity experiments were performed. Briefly, TCPP or INMs were incubated in MCF-7 cells for 4 h, removed, and exposed to visible lamp light (0.14 W/cm^2, 10 min). For the control, cells were left in the dark. Afterward, the cells were incubated an additional 24 h, and the cell viability was determined by the MTT assay. TCPP displays no dark toxicity under the concentration range used; however, it shows some toxicity under light irradiation (Figure 5a). $[P_{66614}]_4[TCPP]$ INMs

show similar dark toxicity as that previously determined with an increase in IC_{50} due to a decreased incubation time of 4 h (Figure 5b). However, under light irradiation, INMs exhibit high light toxicity (Table S1). The increased cytotoxicity of porphyrin in INMs in comparison to the parent compound is due to improved photophysical properties such as ROS and singlet oxygen qunatum yield. This study revealed that the INMs approach can be utilized to attain an enhanced PDT effect.

To further explain the mechanism of enhanced cytotoxicity of INMs, cellular uptake experiments were performed. Briefly, TCPP and INMs were separately incubated in a six-well plate for 4 h. Afterward, the cells were washed thoroughly with PBS and dissolved with 100% DMSO solution. A spectrophotometer was used to determine the concentration of the dissolved drug. It was found that INMs were uptaken by cells 1.5 times more than TCPP after 4 h (Figure 6). This shows that INMs exhibit an enhanced cytotoxicity due to the greater uptake by MCF-7 cells because of the NP morphology, improved photophysical properties, as well as dual mechanisms (chemotherapy along with PDT) present in a single nanodrug.

4. CONCLUSION

A facile one-step metathesis reaction was used to synthesize chemo–PDT combination IMs for cancer therapy application for the first time. INMs are simply prepared using a repreicipitation method without adding any matrix. Conversion to IM reduced the planar face aggregation of the porphyrin units, thus shifting its wavelength maxima to a longer wavelength, which is important for deeper light penetration for PDT. The phosphorescence emission intensity of TCPP is enhanced upon conversion to IM along with the excited-state lifetime, which improved the PDT performance of the porphyrin anion in the combination drug. The ROS quantum yield doubled in value for the IM as compared to that of TCPP, which is expected due to the long triplet state lifetime and the reduced aggregation as compared to those of the free porphyrin. Also, INMs displayed enhanced dark toxicity toward cancerous cells due to the enhanced cellular uptake of the NPs-based combination drug. Further, due to their superior singlet oxygen production and light toxicity as compared to TCPP, $[P_{66614}]_4[TCPP]$ INMs show great potential as an all-in-one combination anticancer drug that is of low-cost and is simple to produce. Furthermore, the INMs' surface is functionalized with FA using simple ionic interactions, which aid to tune the selectivity of the INMs toward cancer cells. The beauty in IL chemistry is the ease in tunability as there are many different cytotoxic and photosensitizing combinations possible to finely design a drug for the desired effects in vitro.

Supplementary Material

Refer to Web version on PubMed Central for supplementary material.

Funding

in this material are those of the author(s) and do not necessarily reflect the views of the National Science Foundation.

ABBREVIATIONS

PDT	photodynamic therapy
FA	folic acid
TCPP	*meso*-tetra(4-carboxyphenyl)porphyrin
INM	ionic nanomaterial
PS	photosensitizer
NP	nanoparticle
ABDA	9,10-anthracenediyl-bis(methylene)dimalonic acid
DPBF	1,3-diphenylisobenzofuran
ROS	reactive oxygen species

REFERENCES

(1). Siegel RL; Miller KD; Jemal A Cancer Statistics, 2020. Ca-Cancer J. Clin 2020, 70 (1), 7–30. [PubMed: 31912902]

(2). Hwang HS; Shin H; Han J; Na K Combination of Photodynamic Therapy (PDT) and Anti-Tumor Immunity in Cancer Therapy. J. Pharm. Invest 2018, 48 (2), 143–151.

(3). Wentrup R; Winkelmann N; Mitroshkin A; Prager M; Voderholzer W; Schachschal G; Jürgensen C; Büning C Photodynamic Therapy plus Chemotherapy Compared with Photodynamic Therapy Alone in Hilar Nonresectable Cholangiocarcinoma. Gut Liver 2016, 10 (3), 470–475. [PubMed: 26814610]

(4). Hou W; Zhao X; Qian X; Pan F; Zhang C; Yang Y; De La Fuente JM; Cui D PH-Sensitive Self-Assembling Nanoparticles for Tumor near-Infrared Fluorescence Imaging and Chemo-Photodynamic Combination Therapy. Nanoscale 2016, 8 (1), 104–116. [PubMed: 26607263]

(5). Ryan Q; Ibrahim A; Cohen MH; Johnson J; Ko C; Sridhara R; Justice R; Pazdur R FDA Drug Approval Summary: Lapatinib in Combination with Capecitabine for Previously Treated Metastatic Breast Cancer That Overexpresses HER-2. Oncologist 2008, 13 (10), 1114–1119. [PubMed: 18849320]

(6). Blagosklonny MV Analysis of FDA Approved Anticancer Drugs Reveals the Future of Cancer Therapy. Cell Cycle 2004, 3 (8), 1035–1042. [PubMed: 15254418]

(7). Cheng Z; Al Zaki A; Hui JZ; Muzykantov VR; Tsourkas A Multifunctional Nanoparticles: Cost versus Benefit of Adding Targeting and Imaging Capabilities. Science (Washington, DC, U. S.) 2012, 338 (6109), 903–910.

(8). Zhou J; Lu Z; Zhu X; Wang X; Liao Y; Ma Z; Li F NIR Photothermal Therapy Using Polyaniline Nanoparticles. Biomaterials 2013, 34 (37), 9584–9592. [PubMed: 24044996]

(9). Lee JH; Nan A Combination Drug Delivery Approaches in Metastatic Breast Cancer. J. Drug Delivery 2012, 2012, 1–17.

(10). Warner IM; El-Zahab B; Siraj N Perspectives on Moving Ionic Liquid Chemistry into the Solid Phase. Anal. Chem 2014, 86 (15), 7184–7191. [PubMed: 25017178]

(11). Siraj N; Hasan F; Das S; Kiruri LW; Steege Gall KE; Baker GA; Warner IM J. Phys. Chem. C 2014, 118 (5), 2312–2320.

(12). Siraj N; Das S; Hasan F; Lu C; Kiruri LW; Steege Gall KE; Warner IM Enhanced S2 Emission in Carbazole-Based Ionic Liquids. RSC Adv. 2015, 5 (13), 9939–9945.

(13). Siraj N; Magut PKS; Mcdonough K; Sahasrabudhe G; Warner IM Mol. Pharmaceutics 2018, 15 (9), 3837–3845.

(14). Kolic PE; Siraj N; Cong M; Regmi BP; Luan X; Wang Y; Warner IM Improving Energy Relay Dyes for Dye-Sensitized Solar Cells by Use of a Group of Uniform Materials Based on Organic Salts (GUMBOS). RSC Adv. 2016, 6 (97), 95273–95282.

(15). Macchi S; Zubair M; Ali N; Guisbiers G; Siraj N Tunable Cytotoxicity and Selectivity of Phosphonium Ionic Liquid with Aniline Blue Dye. J. Nanosci. Nanotechnol 2021, 21 (12), 6143–6150. [PubMed: 34229815]

(16). Le T; Macchi S; Jalihal A; Szwedo S; Siraj N Paper-Based Portable Sensor and Nanosensor For Sulfur Dioxide Detection. Curr. Res. Mater. Chem 2021, 3, 109.

(17). Berton P; Siraj N; Das S; de Rooy S; Wuilloud RG; Warner IM Efficient Low-Cost Procedure for Microextraction of Estrogen from Environmental Water Using Magnetic Ionic Liquids. Molecules 2021, 26 (1), 32.

(18). Kumar V; Malhotra SV Antitumor Activity of Ionic Liquids on Human Tumor Cell Lines. ACS Symposium Series; UTC, 2010; Vol. 1038, pp 91–102.

(19). Kumar V; Malhotra SV Bioorganic & Medicinal Chemistry Letters Study on the Potential Anti-Cancer Activity of Phosphonium and Ammonium-Based Ionic Liquids. Bioorg. Med. Chem. Lett 2009, 19 (16), 4643–4646. [PubMed: 19615902]

(20). Moodley KG Roles of Ionic Liquids in Medicines for the Treatment of Cancer and Tuberculosis. Der Pharma Chem. 2019, 11, 1–19.

(21). Hough WL; Smiglak M; Rodríguez H; Swatloski RP; Spear SK; Daly DT; Pernak J; Grisel JE; Carliss RD; Soutullo MD; Davis JH; Rogers RD The Third Evolution of Ionic Liquids: Active Pharmaceutical Ingredients. New J. Chem 2007, 31 (8), 1429–1436.

(22). Master A; Livingston M; Sen Gupta A Photodynamic Nanomedicine in the Treatment of Solid Tumors: Perspectives and Challenges. J. Controlled Release 2013, 168 (1), 88–102.

(23). Kruger CA; Abrahamse H Utilisation of Targeted Nanoparticle Photosensitiser Drug Delivery Systems for the Enhancement of Photodynamic Therapy. Molecules 2018, 23, 2628.

(24). Hu C-MJ; Aryal S; Zhang L Nanoparticle-Assisted Combination Therapies for Effective Cancer Treatment. Ther. Delivery 2010, 1 (2), 323–334.

(25). Bae KH; Chung HJ; Park TG Nanomaterials for Cancer Therapy and Imaging. Mol. Cells 2011, 31 (4), 295–302. [PubMed: 21360197]

(26). Onoue S; Yamada S; Chan HK Nanodrugs: Pharmacokinetics and Safety. Int. J. Nanomed 2014, 9 (1), 1025–1037.

(27). Zhang R; Xing R; Jiao T; Chen C; Ma K; Ma G; Yan X Carrier-Free, Chemophotodynamic Dual Nanodrugs via Self-Assembly for Synergistic Antitumor Therapy. ACS Appl. Mater. Interfaces 2016, 8 (21), 13262–13269. [PubMed: 27176934]

(28). Cuenca AG; Jiang H; Hochwald SN; Delano M; Cance WG; Grobmyer SR Emerging Implications of Nanotechnology on Cancer Diagnostics and Therapeutics. Cancer 2006, 107 (3), 459–466. [PubMed: 16795065]

(29). Diaz-Uribe CE; Daza MC; Páez-Mozo EA; Martínez O,F; Guedes CLB; Di Mauro E Visible Light Singlet Oxygen Production with Tetra(4-Carboxyphenyl) Porphyrin/SiO2. J. Photochem. Photobiol., A 2013, 259, 47–52.

(30). Debele TA; Peng S; Tsai HC Drug Carrier for Photodynamic Cancer Therapy. Int. J. Mol. Sci 2015, 16 (9), 22094–22136. [PubMed: 26389879]

(31). Miao W; Kim H; Gujrati V; Kim JY; Jon H; Lee Y; Choi M; Kim J; Lee S; Lee DY; Kang S; Jon S Photo-Decomposable Organic Nanoparticles for Combined Tumor Optical Imaging and Multiple Phototherapies. Theranostics 2016, 6 (13), 2367–2379. [PubMed: 27877241]

(32). Sun X; Zebibula A; Dong X; Li G; Zhang G; Zhang D; Qian J; He S Targeted and Imaging-Guided in Vivo Photodynamic Therapy for Tumors Using Dual-Function, Aggregation-Induced Emission Nanoparticles. Nano Res. 2018, 11 (5), 2756–2770.

(33). Rui LL; Cao HL; Xue YD; Liu LC; Xu L; Gao Y; Zhang WA Functional Organic Nanoparticles for Photodynamic Therapy. Chin. Chem. Lett 2016, 27 (8), 1412–1420.

(34). Hong EJ; Choi DG; Shim MS Targeted and Effective Photodynamic Therapy for Cancer Using Functionalized Nanomaterials. Acta Pharm. Sin. B 2016, 6 (4), 297–307. [PubMed: 27471670]

(35). Van Vlerken LE; Vyas TK; Amiji MM Poly(Ethylene Glycol)-Modified Nanocarriers for Tumor-Targeted and Intracellular Delivery. Pharm. Res 2007, 24 (8), 1405–1414. [PubMed: 17393074]

(36). Chen C; Ke J; Edward Zhou X; Yi W; Brunzelle JS; Li J; Yong EL; Xu HE; Melcher K Structural Basis for Molecular Recognition of Folic Acid by Folate Receptors. Nature 2013, 500 (7463), 486–489. [PubMed: 23851396]

(37). Cheung A; Bax HJ; Josephs DH; Ilieva KM; Pellizzari G; Opzoomer J; Bloomfield J; Fittall M; Grigoriadis A; Figini M; Canevari S; Spicer JF; Tutt AN; Karagiannis SN Targeting Folate Receptor Alpha for Cancer Treatment. Oncotarget 2016, 7 (32), 52553–52574. [PubMed: 27248175]

(38). Lin Y; Zhou T; Bai R; Xie Y Chemical Approaches for the Enhancement of Porphyrin Skeleton-Based Photodynamic Therapy. J. Enzyme Inhib. Med. Chem 2020, 35 (1), 1080–1099. [PubMed: 32329382]

(39). Liu S; Hu Y; Hu C; Xiong Y; Duan M Quantum Yields of Singlet Oxygen of Tetrakis (4-Carboxyphenyl) Porphyrin in Different Solvents. J. Porphyrins Phthalocyanines 2019, 23, 1–8.

(40). Mosinger J; Deumié M; Lang K; Kubát P; Wagnerová DM Supramolecular Sensitizer: Complexation of Meso-Tetrakis(4-Sulfonatophenyl)Porphyrin with 2-Hydroxypropyl-Cyclodextrins. J. Photochem. Photobiol., A 2000, 130 (1), 13–20.

(41). Kolic PE; Siraj N; Hamdan S; Regmi BP; Warner IM Synthesis and Characterization of Porphyrin-Based GUMBOS and NanoGUMBOS as Improved Photosensitizers. J. Phys. Chem. C 2016, 120 (9), 5155–5163.

(42). Siraj N; Kolic PE; Regmi BP; Warner IM Strategy for Tuning the Photophysical Properties of Photosensitizers for Use in Photodynamic Therapy. Chem. - Eur. J 2015, 21 (41), 14440–14446. [PubMed: 26288164]

(43). Li M; Yu C; Hu C; Yang W; Zhao C; Wang S; Zhang M; Zhao J; Wang X; Qiu J Solvothermal Conversion of Coal into Nitrogen-Doped Carbon Dots with Singlet Oxygen Generation and High Quantum Yield. Chem. Eng. J 2017, 320, 570–575.

(44). Kilaparty SP; Agarwal R; Singh P; Kannan K; Ali N Endoplasmic Reticulum Stress-Induced Apoptosis Accompanies Enhanced Expression of Multiple Inositol Polyphosphate Phosphatase 1 (Minpp1): A Possible Role for Minpp1 in Cellular Stress Response. Cell Stress Chaperones 2016, 21 (4), 593–608. [PubMed: 27038811]

(45). Lambert CR; Reddi E; Spikes JD; Rodgers MAJ; Jori G The Effects of Porphyrin Structure and Aggregation State on Photosensitized Processes in Aqueous and Micellar Media. Photochem. Photobiol 1986, 44 (5), 595–601. [PubMed: 3809256]

(46). Kano K; Fukuda K; Wakami H; Nishiyabu R; Pasternack RF Factors Influencing Self-Aggregation Tendencies of Cationic Porphyrins in Aqueous Solution. J. Am. Chem. Soc 2000, 122 (31), 7494–7502.

(47). Friesen B An Investigation of Porphyrin Aggregation Using Spectroscopic and Microscopic Methods. Ph.D. Thesis, 2011; p 1.

(48). Pasternack RF; Fleming C; Herring S; Collings PJ; DePaula J; DeCastro G; Gibbs EJ Aggregation Kinetics of Extended Porphyrin and Cyanine Dye Assemblies. Biophys. J 2000, 79 (1), 550–560. [PubMed: 10866980]

(49). Zhang DW; Chen WT Two Novel Tcpp Porphyrinic Compounds: In Situ Syntheses, Characterization and Reaction Mechanism. J. Chil. Chem. Soc 2017, 62 (1), 3381–3385.

(50). Hoche J; Schulz A; Dietrich LM; Humeniuk A; Stolte M; Schmidt D; Brixner T; Würthner F; Mitric R The Origin of the Solvent Dependence of Fluorescence Quantum Yields in Dipolar Merocyanine Dyes. Chem. Sci 2019, 10 (48), 11013–11022. [PubMed: 32206253]

(51). Ho-Wu R; Yau SH; Goodson T Efficient Singlet Oxygen Generation in Metal Nanoclusters for Two-Photon Photodynamic Therapy Applications. J. Phys. Chem. B 2017, 121 (43), 10073–10080. [PubMed: 29016137]

(52). Marin DM; Payerpaj S; Collier GS; Ortiz AL; Singh G; Jones M; Walter MG Efficient Intersystem Crossing Using Singly Halogenated Carbomethoxyphenyl Porphyrins Measured Using Delayed Fluorescence, Chemical Quenching, and Singlet Oxygen Emission. Phys. Chem. Chem. Phys 2015, 17 (43), 29090–29096. [PubMed: 26460933]

(53). Spiller W; Kliesch H; Wöhrle D; Hackbarth S; Röder B; Schnurpfeil G Singlet Oxygen Quantum Yields of Different Photo-Sensitizers in Polar Solvents and Micellar Solutions. J. Porphyrins Phthalocyanines 1998, 2 (2), 145–158.

(54). Schmitz C; Aubry JM; Rigaudy J A New Access to the Anthracene Core. Synthesis of Two Water Soluble Singlet Oxygen Traps Derived from 1,3-Diphenylisobenzofuran and 9,10-Diphenylan-thracene. Tetrahedron 1982, 38 (10), 1425–1430.

(55). Tanielian C; Schweitzer C; Mechin R; Wolff C Quantum Yield of Singlet Oxygen Production by Monomeric and Aggregated Forms of Hematoporphyrin Derivative. Free Radical Biol. Med 2001, 30 (2), 208–212. [PubMed: 11163538]

(56). Entradas T; Waldron S; Volk M The Detection Sensitivity of Commonly Used Singlet Oxygen Probes in Aqueous Environments. J. Photochem. Photobiol., B 2020, 204, 111787. [PubMed: 31958676]

(57). Kelemen LE The Role of Folate Receptor α in Cancer Development, Progression and Treatment: Cause, Consequence or Innocent Bystander? Int. J. Cancer 2006, 119 (2), 243–250. [PubMed: 16453285]

(58). Leamon CP; Low PS Delivery of Macromolecules into Living Cells: A Method That Exploits Folate Receptor Endocytosis. Proc. Natl. Acad. Sci. U. S. A 1991, 88 (13), 5572–5576. [PubMed: 2062838]

(59). Gao JQ; Eto Y; Yoshioka Y; Sekiguchi F; Kurachi S; Morishige T; Yao X; Watanabe H; Asavatanabodee R; Sakurai F; Mizuguchi H; Okada Y; Mukai Y; Tsutsumi Y; Mayumi T; Okada N; Nakagawa S Effective Tumor Targeted Gene Transfer Using PEGylated Adenovirus Vector via Systemic Administration. J. Controlled Release 2007, 122 (1), 102–110.
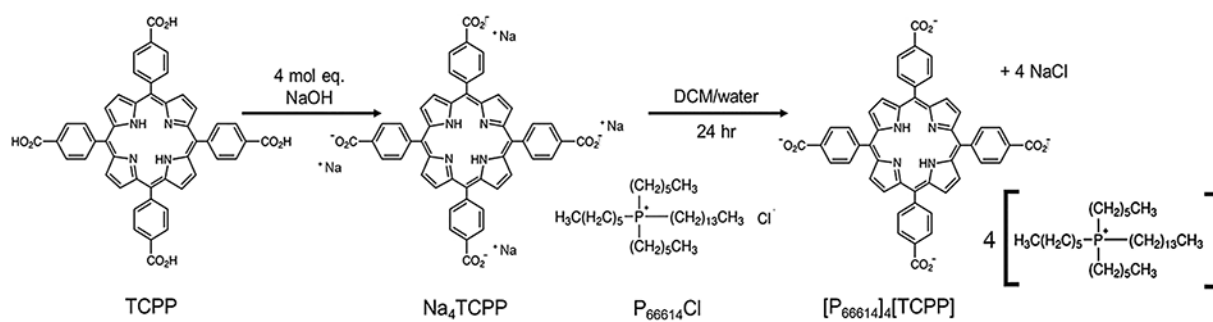
Figure 1.
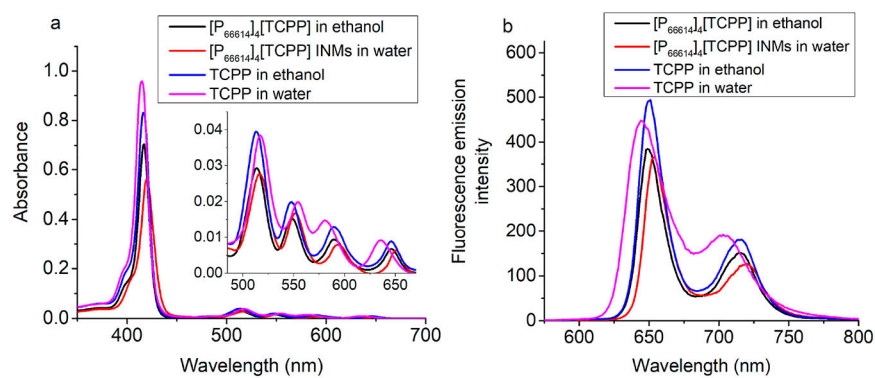Scheme of the IMs combination drug synthesis.

Figure 2.
(a) Absorption spectra and (b) fluorescence emission spectra of 2.5 μM dye samples/ INMs in water and in ethanol at an excitation wavelength maximum for each sample of approximately 420 nm.
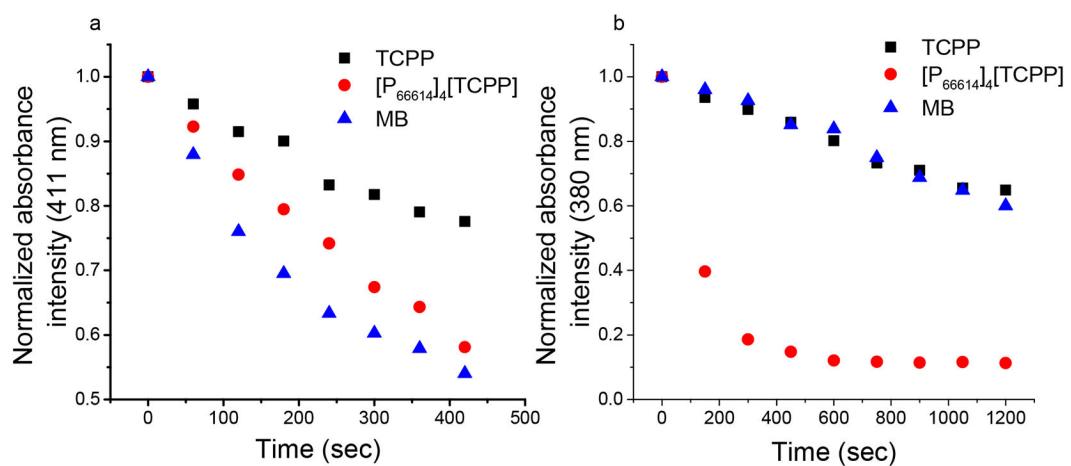
Figure 3.
Photodegradation of (a) DPBF and (b) ABDA upon increasing irradiation time in the presence of TCPP, [P$_{66614}$]$_4$[TCPP], and MB. The final drug concentrations were 5 and 10 μM with DPBF and ABDA, respectively.
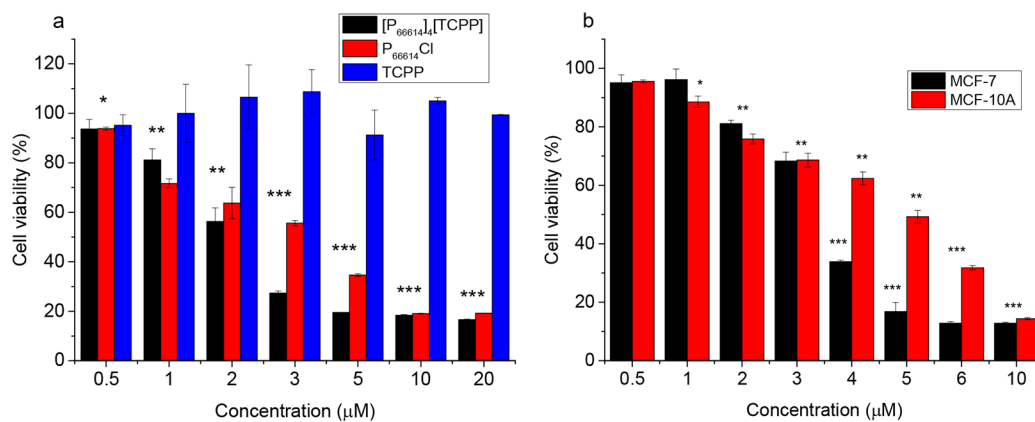
Figure 4.
Cell viability of (a) MCF-7 cells upon dosage with varying concentrations of combination INMs and parent compounds (0.5–20 μM) for 24 h and (b) FA-coated INMs incubated in cancer (MCF-7) and noncancerous (MCF-10A) cell lines for 24 h at a concentration range of 0.5–10 μM (*$p < 0.05$, **$p < 0.01$, ***$p < 0.005$).
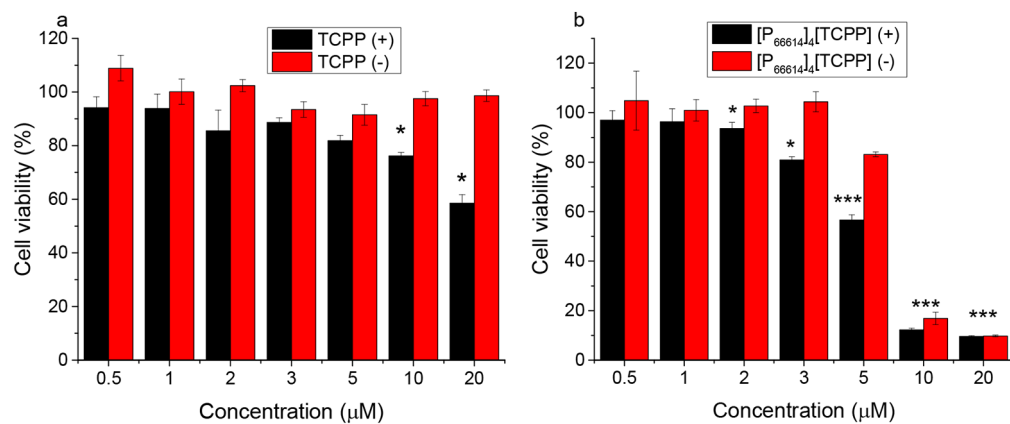
Figure 5.
Toxicity of (a) TCPP and (b) $[P_{66614}]_4[TCPP]$ INMs after 4 h of incubation in MCF-7 cells under light irradiation, 0.14 W/cm^2 (+), or in the dark (−) at a concentration range of 0.5–20 μM (*$p < 0.05$, **$p < 0.01$, ***$p < 0.005$).
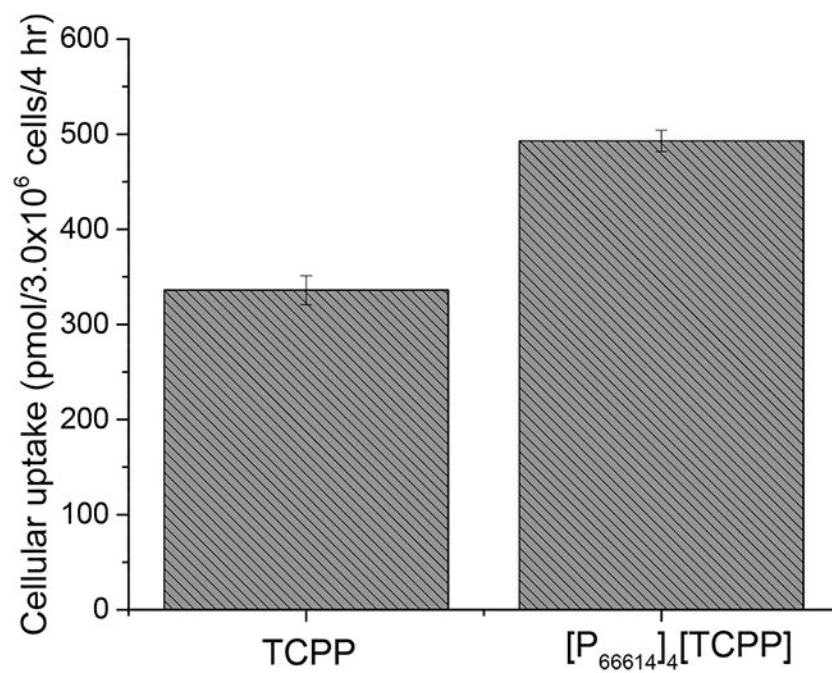
Figure 6.
Cellular uptake of TCPP and INMs in MCF-7 cells after incubation of 4 nmol of drug for 4 h.

Table 1.

Molar Absorptivity of Compounds in Water and Ethanol Solvents

compound	λ_{max} (nm)	ε (L mol^{-1} cm^{-1})
TCPP in water	415, 517, 555, 580, 635	1.40×10^5, 5.52×10^3, 2.81×10^3, 2.09×10^3, 1.28×10^3
[P$_{66614}$]$_4$[TCPP] INMs in water	420, 516, 552, 593, 649	9.10×10^4, 3.98×10^3, 2.35×10^3, 1.12×10^3, 0.90×10^3
TCPP in ethanol	417, 514, 548, 588, 645	1.21×10^5, 5.69×10^3, 2.83×10^3, 1.77×10^3, 1.22×10^3
[P$_{66614}$]$_4$[TCPP] IMs in ethanol	417, 513, 548, 588, 645	1.02×10^5, 4.11×10^3, 2.13×10^3, 1.31×10^3, 0.85×10^3

Table 2.

Fluorescence Quantum Yield and Radiative/Nonradiative Rates of Compounds

compound	Φ_F	$k_{rad}/s^{-1} \times 10^6$	$k_{nonrad}/s^{-1} \times 10^7$
TCPP in water	0.058	1.09	2.39
$[P_{66614}]_4$[TCPP] INMs in water	0.050	0.79	1.50
FA-functionalized $[P_{66614}]_4$[TCPP] INMs in water	0.016	0.80	5.04
TCPP in ethanol	0.044[a]	1.10	1.78
$[P_{66614}]_4$[TCPP] in ethanol	0.048	0.80	1.57

[a]This value was obtained from ref 39.

Table 3.

Fluorescence Lifetimes of IM and Parent TCPP in Ethanol Recorded at 390 nm Excitation/650 nm Emission Wavelength

sample	τ_1 (ns)	a_1	τ_2 (ns)	a_2	χ^2
TCPP	1.06	0.045	9.47	0.954	1.14
[P$_{66614}$]$_4$[TCPP]	0.57	0.043	10.52	0.957	1.23

Table 4.

ROS/Singlet Oxygen Quantum Yield Values Obtained for Each PS in Ethanol or Water Solvent

solvent/probe	MB	TCPP	$[P_{66614}]_4[TCPP]$
ethanol/DPBF	0.52	0.14	0.28 (IM)
water/ABDA	0.52	0.19	0.97 (INMs)

Table 5.

Calculated IC$_{50}$ Concentrations (μM) of Drugs in Different Cell Lines at 10^4 Cells per Well after 24 h in the Dark

cell line	IC$_{50}$ concentration (μM)		
	P$_{66614}$Cl	[P$_{66614}$]$_4$[TCPP] INMs	FA-[P$_{66614}$]$_4$[TCPP] INMs
MCF-7	3.39 ± 0.21	1.94 ± 0.15	3.25 ± 0.18
MCF-10A	3.28 ± 0.12	1.53 ± 0.13	5.20 ± 0.15